PERTURBATION TECHNIQUE FOR WAVE PROPAGATION ANALYSIS IN A NOTCHED BEAM USING WAVELET SPECTRAL ELEMENT MODELING

Mira Mitra, S. Gopalakrishnan, Massimo Ruzzene, Nicole Apetre and S. Hanagud

PERTURBATION TECHNIQUE FOR WAVE PROPAGATION ANALYSIS IN A NOTCHED BEAM USING WAVELET SPECTRAL ELEMENT MODELING

MIRA MITRA, S. GOPALAKRISHNAN, MASSIMO RUZZENE, NICOLE APETRE AND S. HANAGUD

In this paper, spectral finite element is formulated for an Euler–Bernoulli beam with through-width notch type defect. In spectral finite element modeling, exact shape functions are derived and finite element procedure is followed in the transformed frequency domain. Here spectral finite element formulation is done using Daubechies scaling function bases for temporal approximation. In comparison to the conventional Fourier transform based spectral finite element method, the use of localized bases functions in the Daubechies scaling function based spectral finite element method allows accurate wave propagation analysis of finite length structures. The wave propagation response of the damaged beam is considered as a perturbation of the undamaged beam response within the restriction of small damage. First, numerical experiments are performed with narrow banded modulated pulse loading to obtain the location of damage from wave arrival time. Next, a broad banded impulse load is considered and effects of parameters like damage width, depth, and location on the responses are studied in time and frequency domains.

1. Introduction

Diagnostic waves are extensively used for structural health monitoring. Wave propagation problems deal with high frequency excitations and thus help to identify the presence of very small damages. These wave based techniques can thus be used to detect the minute defects which occur at the onset of the damage, and then propagate, causing failure of the structure.

Numerical solution of wave equations requires high accuracy in numerical differentiation and, for computational efficiency, it needs to have larger spatial grids and time steps. The conventional finite element (FE) technique widely used for modeling of structures is not suitable here, mainly because the element size should be comparable to the wavelength, which is very small at higher frequencies. This makes FE modeling computationally prohibitive for wave propagation problems. Alternative numerical techniques are generally adopted for such problems, and fast Fourier transform-based spectral finite element (FSFE) [Doyle 1999] is one such method. In short, the method follows FE technique in the transformed frequency domain. The governing partial differential equations are reduced to ordinary differential equations (ODEs) using fast Fourier transform (FFT) in time. These ODEs are solved exactly to derive the shape functions which are used to obtain the elemental dynamic stiffness matrix relating the transformed nodal forces and displacements.

However, the FSFE method possesses certain serious limitations as it uses bases with global support for temporal approximation, and thus requires the assumption of periodicity. As a consequence, the FSFE method does not allow time domain analysis of wave propagation in finite length structures. This problem is referred as "wrap around". To eliminate this drawback of FSFE, a Daubechies scaling function based

---

spectral finite element, referred to as a wavelet based spectral finite element [Mitra and Gopalakrishnan 2005] (WSFE), is formulated using compactly supported Daubechies scaling as bases for approximation in time. The localized nature of the basis functions allows accurate simulation of wave propagation in finite length waveguides. In addition, similar to FSFE, the present method is computationally efficient and allows simultaneous frequency domain analysis [Mitra and Gopalakrishnan 2006].

In this paper, WSFE is formulated for a notched Euler–Bernoulli beam. The effect of the notch is introduced in the formulation using perturbation technique. The wave propagation response of the damaged beam is considered to be a perturbation of the response of the undamaged beam with the assumption of small damage. This perturbation technique has been developed to identify the presence of damage in beam [Luo and Hanagud 1998] and plates [Sharma et al. 2006] using curvature as the indicator; the effect of the notch on the curvature is studied using modal analysis. It should be mentioned here that as the analysis is restricted to damages with much smaller dimension, compared to that of the beam, the mode conversion resulting in axial and flexural coupling is not considered in the formulation. The present method is developed for pure flexural wave propagation and the effect of axial coupling due to the presence of the notch is neglected.

The paper is organized as follows. In Section 2, a brief overview of Daubechies compactly supported wavelets is provided. In the next two sections, the reduction of the wave equations and the perturbation techniques are elaborated. Section 5 concisely describes the spectral finite element formulation. Numerical experiments are presented in Section 6. The examples are provided for an aluminum cantilever beam with through-width notches of different configurations. The effects of the presence of the notch on the wave propagation responses due to both narrow and broad banded loading are studied in time and frequency domains. The influences of damage parameters like width, depth, and location on the responses are also analyzed.

2. Daubechies compactly supported wavelets

A concise review of the orthogonal bases of Daubechies wavelets [Daubechies 1992] is provided. Wavelets $\psi_{j,k}(t)$ form compactly supported orthonormal bases for $L^2(R)$. The wavelets and the associated scaling functions $\varphi_{j,k}(t)$ are obtained by translation and dilation of single functions $\psi(t)$ and $\varphi(t)$, respectively, as

$$\psi_{j,k}(t) = 2^{j/2}\psi(2^j t - k), \qquad j, k \in \mathbf{Z},$$
$$\varphi_{j,k}(t) = 2^{j/2}\varphi(2^j t - k), \qquad j, k \in \mathbf{Z}.$$

The scaling functions $\varphi(t)$ are derived from the dilation or scaling equation

$$\varphi(t) = \sum_k a_k \varphi(2t - k), \qquad (1)$$

and the wavelet function $\psi(t)$ is obtained as

$$\psi(t) = \sum_k (-1)^k a_{1-k} \varphi(2t - k). \qquad (2)$$

a_k are the filter coefficients, and they are fixed for specific wavelet or scaling function bases. For compactly supported wavelets only a finite number of a_k are nonzero. The filter coefficients a_k are derived by

imposing certain constraints on the scaling functions, which are as follows: First, the area under scaling function is normalized to one. Second, the scaling function $\varphi(t)$ and its translates are orthonormal. Finally, the wavelet function $\psi(t)$ has M vanishing moments. The number of vanishing moments M denotes the order N of the Daubechies wavelet, where $N = 2M$.

Let $P_j(f)(t)$ be the approximation of a function $f(t)$ in $\mathbf{L}^2(\mathbf{R})$, using $\varphi_{j,k}(t)$ as bases, at a certain level (resolution) j, then

$$P_j(f)(t) = \sum_k c_{j,k}\varphi_{j,k}(t), \qquad k \in \mathbf{Z}, \tag{3}$$

where $c_{j,k}$ are the approximation coefficients.

3. Reduction of wave equations to ODEs

The governing differential equations for a Euler–Bernoulli beam are given as

$$EI\frac{\partial^4 w}{\partial x^4} + \rho A\frac{\partial^2 w}{\partial t^2} = 0, \tag{4}$$

where $w(x, t)$ is the transverse displacement. E and ρ are the Young's modulus and mass density, respectively, and I and A are area moment of inertia and area, respectively. The associated force boundary conditions are

$$EI\frac{\partial^2 w}{\partial x^2} = M \qquad \text{and} \qquad EI\frac{\partial^3 w}{\partial x^3} = -V, \tag{5}$$

where M and V are respectively the applied moment and the transverse force.

The first step of formulation of WSFE is the reduction of the governing differential equation given by Equation (4) to a set of coupled ODEs by Daubechies scaling function based transformation in time [Mitra and Gopalakrishnan 2005]. The procedure is described here in brief, for completeness. Let $w(x, t)$ be discretized at n points in the time window $[0, t_f]$. Let $\tau = 0, 1, \ldots, n-1$ be the sampling points, then $t = \triangle t \, \tau$, where $\triangle t$ is the time interval between two sampling points. The function $w(x, t)$ can be approximated a by scaling function $\varphi(\tau)$ at an arbitrary scale as

$$w(x, t) = w(x, \tau) = \sum_k w_k(x)\varphi(\tau - k), \qquad k \in \mathbf{Z},$$

where $w_k(x)$ (referred to as w_k hereafter) is the approximation coefficient at a certain spatial dimension x. Thus (4) can be written as

$$EI\sum_k \frac{d^4 w_k}{dx^4}\varphi(\tau - k) + \frac{\rho A}{\triangle t^2}\sum_k w_k\varphi''(\tau - k) = 0. \tag{6}$$

Taking the inner product of both sides of (6) with the translates of scaling functions $\varphi(\tau - j)$, where $j = 0, 1, \ldots, n-1$, and using their orthogonal properties, we get n simultaneous ODEs as

$$EI\frac{d^4 w_j}{dx^4} + \frac{\rho A}{\triangle t^2}\sum_{k=j-N+2}^{j+N-2}\Omega^2_{j-k}w_k = 0, \qquad j = 0, 1, \ldots, n-1, \tag{7}$$

where N is the order of the Daubechies wavelet, and the connection coefficients for the n-th order derivative are defined as

$$\Omega^n_{j-k} = \int \varphi^n(\tau - k)\varphi(\tau - j)\,d\tau.$$

For compactly supported wavelets, the first and second order connection coefficients, Ω^1_{j-k} and Ω^2_{j-k}, are nonzero only in the interval $k = j - N + 2$ to $k = j + N - 2$. The details for evaluation of the connection coefficients for different orders of the derivative are given by Beylkin [1992].

It can be observed from the ODEs given by Equation (7) that certain coefficients w_j near the vicinity of the boundaries ($j = 0$ and $j = n - 1$) lie outside the time window $[0, t_f]$ defined by $j = 0, 1, \ldots, n - 1$. These coefficients must be treated properly for finite domain analysis; the wavelet based extrapolation scheme [Williams and Amaratunga 1997] is implemented for this purpose. The above method converts the ODEs given by (7) to a set of coupled ODEs given as

$$EI \left\{ \frac{d^4 w_j}{dx^4} \right\} + \left[\Gamma^1 \right]^2 \rho A \{w_j\} = 0, \tag{8}$$

where Γ^1 is the first order connection coefficient matrix obtained after using the wavelet extrapolation technique. It should be mentioned here that though the connection coefficients matrix, Γ^2, for the second order derivative can be obtained independently, here it is written as $\left[\Gamma^1 \right]^2$, as it helps to impose the initial conditions [Mitra and Gopalakrishnan 2005]. These coupled ODEs are decoupled using eigenvalue analysis as $\Gamma^1 = \Phi \Pi \Phi^{-1}$, where Π is the diagonal eigenvalue matrix and Φ is the eigenvectors matrix of Γ^1. Let the eigenvalues be $\iota \gamma_j$ ($\iota = \sqrt{-1}$), then the decoupled ODEs corresponding to (8) are

$$EI \frac{d^4 \hat{w}_j}{dx^4} - \rho A \gamma_j^2 \, \hat{w}_j = 0, \qquad j = 0, 1, \ldots, n - 1, \tag{9}$$

where $\hat{w}_j$ is defined as $\hat{w}_j = \Phi^{-1} w_j$.

Similarly, the transformed form of the force boundary conditions given by (5) are given as

$$EI \frac{d^2 \hat{w}_j}{dx^2} = \hat{M}_j, \qquad EI \frac{d^3 \hat{w}_j}{dx^3} = -\hat{V}_j, \qquad j = 0, 1, \ldots, n - 1, \tag{10}$$

where $\hat{M}_j$ and $\hat{V}_j$ are the transformed $M(x, t)$ and $V(x, t)$, respectively. In the following sections, the subscript j is dropped for simplified notation and all the following equations hold for $j = 0, 1, \ldots, n - 1$.

4. Perturbation analysis of damaged beams

Here, a through-width notch is modeled as a localized decrease in the stiffness and inertia. For a notch of width ΔL and depth h_d, as shown in Figure 1, the area moment of inertia I_d at the damaged location can be written as

$$I_d = \frac{1}{12} b(h - h_d)^3 = \frac{1}{12} bh^3 \left(1 - \frac{h_d}{h} \right)^3, \tag{11}$$

where b and h are the width and depth of the beam, respectively. Assuming small damage, meaning $\frac{h_d}{h} \ll 1$, the above Equation (11) can be written as

$$I_d \approx \frac{1}{12} bh^3 \left(1 - 3\frac{h_d}{h} \right) \approx I_0 \left(1 - \epsilon_p \right), \qquad \epsilon_p = 3\frac{h_d}{h},$$
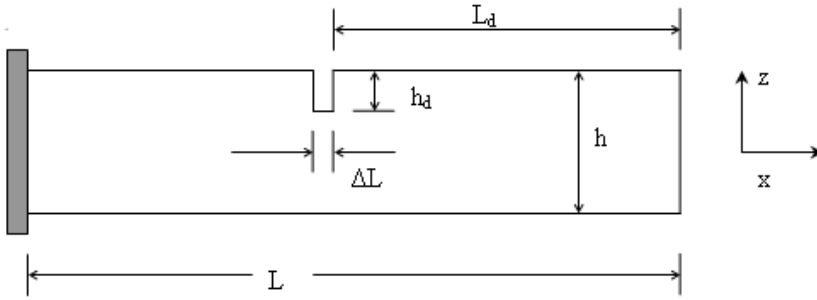
Figure 1. Schematic for the cantilever beam with notch.

where I_0 is the area moment of inertia of the undamaged beam and ϵ_p is used as the perturbation parameter later. Similarly, the mass per unit length at the damaged location, m_d, can be written as

$$m_d = \rho b\left(h - h_d\right) = \rho bh\left(1 - \frac{h_d}{h}\right) = m_0\left(1 - \frac{1}{3}\epsilon_p\right),$$

where m_0 is the mass per unit length of the undamaged beam. Thus, the overall flexural rigidity $EI(x)$ and mass per unit length $m(x)$ of the beam with a notch of width ΔL, at $x = x_d$, can be written as a function of x [Luo and Hanagud 1998]

$$
\begin{aligned}
EI(x) &= EI_0\left[1 - \epsilon_p\Delta L\delta(x - x_d)\right], \\
m(x) &= m_0\left[1 - \tfrac{1}{3}\epsilon_p\Delta L\delta(x - x_d)\right],
\end{aligned}
\tag{12}
$$

where $\delta(x)$ is the Dirac delta function.

Next, the displacement $w(x, t)$ of the damaged beam is considered as a perturbation of that of the undamaged beam [Luo and Hanagud 1998], and is written as

$$w = w^0 - \epsilon_p w^1, \tag{13}$$

where w^0 is the displacement of the undamaged beam, while w^1 is the first approximation of the perturbation solution. The linear transformations used in the last section can be done for the variables in (13), and the transformed equation can be written as

$$\hat{w} = \hat{w}^0 - \epsilon_p\hat{w}^1. \tag{14}$$

Substituting (12) and (14) into (9), the following equations are obtained:

$$1: \; EI_0\frac{d^4\hat{w}^0}{dx^4} = \gamma^2 m_0\hat{w}^0, \tag{15}$$

$$\epsilon_p: \; EI_0\frac{d^4\hat{w}^1}{dx^4} = \gamma^2 m_0\hat{w}^1 + \frac{1}{3}\gamma^2 m_0\Delta L\delta(x - x_d)\hat{w}_d^0 - EI_0\frac{d^2}{dx^2}\left[\Delta L\delta(x - x_d)\frac{d^2\hat{w}_d^0}{dx^2}\right]. \tag{16}$$

However, the terms associated with ϵ_p^2 are neglected. $\hat{w}_d^0$ and $\frac{d^2\hat{w}_d^0}{dx^2}$ are the values of $\hat{w}^0$ and $\frac{d^2\hat{w}^0}{dx^2}$ at $x = x_d$, respectively. The solution of Equation (15) and the complimentary solution of Equation (16) are obtained through the spectral finite element method described in the next section. Here the particular

solution of (16) is required for spectral element formulation. Due to the discontinuity present in (16) it is difficult to obtain the exact particular solution. Thus, the solution of the static part of (16) is taken as the approximate particular solution, which is of the form,

$$\hat{w}^1 = \Delta L \langle x - x_d \rangle \frac{d^2 \hat{w}^0}{dx^2} - \frac{1}{18} \gamma^2 k^4 \Delta L \langle x - x_d \rangle^3 \hat{w}^0 + \frac{1}{6} C_1 x^3 + \frac{1}{2} C_2 x^2 + C_3 x + C_4,$$

where $k^4 = m_0 / E I_0$ and $\langle \ \rangle$ is the ramp function [Jones 1982; Lestari 2001]. C_1, C_2, C_3 and C_4 are the constants to be calculated from the four boundary conditions as

$$\begin{Bmatrix} \hat{w}_1^1 \\ \frac{d\hat{w}_1^1}{dx} \\ \hat{w}_2^1 \\ \frac{d\hat{w}_2^1}{dx} \end{Bmatrix} = \begin{bmatrix} 0 & 0 & 0 & 1 \\ 0 & 0 & 1 & 0 \\ \frac{L^3}{6} & \frac{L^2}{2} & L & 1 \\ \frac{L^2}{2} & L & 1 & 0 \end{bmatrix} \begin{Bmatrix} C_1 \\ C_2 \\ C_3 \\ C_4 \end{Bmatrix} + \begin{Bmatrix} 0 \\ 0 \\ \Delta L (L - x_d) \frac{d^2 \hat{w}_d^0}{dx^2} - \frac{1}{18} \gamma^2 k^4 \Delta L (L - x_d)^3 \hat{w}_d^0 \\ \Delta L \frac{d^2 \hat{w}_d^0}{dx^2} - \frac{1}{6} \gamma^2 k^4 \Delta L (L - x_d)^2 \hat{w}_d^0 \end{Bmatrix}.$$

The above equation can be rewritten more simply as

$$\{u_e^1\} = [G]\{C\} + \{R\}, \tag{17}$$

where

$$\{u_e^1\} = \{\hat{w}_1^1 \ \frac{d\hat{w}_1^1}{dx} (= \theta_1^1) \hat{w}_2^1 \ \frac{d\hat{w}_2^1}{dx} (= \theta_2^1)\}, \quad \hat{w}_1^1 \equiv \hat{w}^1(0) \frac{d\hat{w}_1^1}{dx} \equiv \frac{d\hat{w}^1(0)}{dx}, \quad \hat{w}_2^1 \equiv \hat{w}^1(L) \frac{d\hat{w}_2^1}{dx} \equiv \frac{d\hat{w}^1(L)}{dx},$$

with L being the length of the beam.

Substituting the particular solution given by Equation (17) in the transformed force boundary conditions, (10), we get

$$\hat{M}^1 = E I_0 \Big[\Delta L \delta(x - x_d) \frac{d^2 \hat{w}_d^0}{dx^2} - \frac{1}{3} \gamma^2 k^4 \Delta L \langle x - x_d \rangle \hat{w}_d^0 + C_1 x + C_2 \Big],$$

$$\hat{V}^1 = - E I_0 \Big[\Delta L \frac{d}{dx} \delta(x - x_d) \frac{d^2 \hat{w}_d^0}{dx^2} - \frac{1}{3} \gamma^2 k^4 \Delta L H(x - x_d) \hat{w}_d^0 + C_1 \Big],$$

where $H(x)$ is the step function. The above equations can be written in matrix form relating boundary forces and constants $\{C\}$ as

$$\begin{Bmatrix} \hat{V}_1^1 \\ \hat{M}_1^1 \\ \hat{V}_2^1 \\ \hat{M}_2^1 \end{Bmatrix} = E I_0 \begin{bmatrix} -1 & 0 & 0 & 0 \\ 0 & 1 & 0 & 0 \\ 1 & 0 & 0 & 0 \\ -L & -1 & 0 & 0 \end{bmatrix} \begin{Bmatrix} C_1 \\ C_2 \\ C_3 \\ C_4 \end{Bmatrix} + E I_0 \begin{Bmatrix} 0 \\ 0 \\ -\frac{1}{3} \gamma^2 k^4 \Delta L \hat{w}_d^0 \\ \frac{1}{3} \gamma^2 k^4 \Delta L (L - x_d) \hat{w}_d^0 \end{Bmatrix},$$

or

$$\{\hat{F}_e^1\} = [\overline{G}]\{C\} + \{\overline{R}\}, \tag{18}$$

where

$$\{F_e^1\} = \{\hat{V}_1^1 \ \hat{M}_1^1 \ \hat{V}_2^1 \ \hat{M}_2^1\}, \quad \hat{V}_1^1 \equiv \hat{V}^1(0), \quad \hat{M}_1^1 \equiv \hat{M}^1(0), \quad \hat{V}_2^1 \equiv \hat{V}^1(L), \quad \hat{M}_2^1 \equiv \hat{M}^1(L).$$

Using Equations (17) and (18), the boundary displacements $\{u_e^1\}$ can be written in terms of forces $\{\hat{F}_e^1\}$ as

$$\{\hat{F}_e^1\} = [\hat{K}^1]\{\hat{u}_e^1\} - [\hat{K}^1]\{R\} + \{\overline{R}\}, \qquad \hat{K}^1] = [\overline{G}][G]^{-1}. \tag{19}$$

However, it should be mentioned here that two spectral elements are required to model the notched beam, and one node is located at the damage position. This is needed to account for the discontinuity of the particular solution at $x = x_d$.

The solutions of Equation (15) and the complimentary solution of (16) using the spectral finite element method described in the next section is of similar form, and relates the boundary (nodal) forces and displacements through a matrix equation. Thus the total perturbed solution $\hat{w}^1$ is obtained by adding the particular solution given by (19) to the complimentary solution.

5. Spectral finite element method

As said earlier, (15) and the complimentary part of (16) are solved for $\hat{w}^0$ and $\hat{w}^1$, respectively, using a spectral finite element technique. Here the method is described in a general form considering $\hat{w}$ as the variable. The degrees of freedom (DOFs) associated with the element formulation are shown in Figure 2. The element has two DOFs per node, which are $\hat{w}$ and $d\hat{w}/dx (= \theta)$. From the previous sections, the set of decoupled ODEs (see (9)) are obtained, and are required to be solved exactly for $\hat{w}$. The actual solutions $w(x, t)$ are obtained using inverse wavelet transform. For finite length data, the wavelet transform and its inverse can be obtained using a transformation matrix [Williams and Amaratunga 1994]. Here, the spectral finite element technique is explained for the decoupled ODEs given by (9).

The exact interpolating functions for an element of length L, obtained by solving (9), are

$$\{\hat{w}(x)\}^T = [R][\Theta]\{a\}, \tag{20}$$

where $[\Theta]$ is a diagonal matrix with the diagonal terms $[e^{-k_1 x}, e^{-k_1(L_X - x)}, e^{-k_2 x},$ and $e^{-k_2(L_X - x)}]$; $[R]$ is a 1×4 amplitude ratio matrix for each set of k_1 and k_2 as $[R] = [\ R_{11} \ \ldots \ \ldots \ R_{14} \ ]$. k_1 and k_2 are obtained by substituting (20) into (9) and posing it as a polynomial eigenvalue problem [Chakraborty and Gopalakrishnan 2005].

Here $\{a\} = \{A, B, C, D\}$ are the unknown coefficients to be determined from transformed nodal displacements $\{\hat{u}_e\}$, where

$$\{\hat{u}_e\} = \{\hat{w}_1 \ d\hat{w}_1/dx \ \hat{w}_2 \ d\hat{w}_2/dx\}, \qquad \hat{w}_1 \equiv \hat{w}(0),$$
$$d\hat{w}_1/dx \equiv d\hat{w}(0)/dx, \qquad \hat{w}_2 \equiv \hat{w}(L),$$
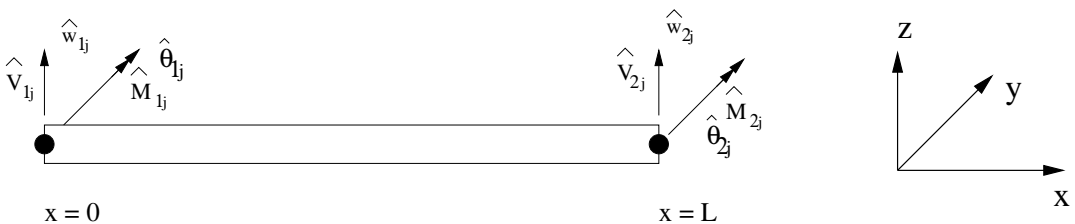

Figure 2. Spectral finite element with nodal displacements and forces.

and $d\hat{w}_2/dx \equiv d\hat{w}/dx(L)$ (see Figure 6 for details on the degrees of freedom the element can support). Thus we can relate the nodal displacements and unknown coefficients as

$$\{\hat{u}_e\} = [B]\{a\}. \tag{21}$$

Substituting Equation (20) in the forced boundary conditions given by (10), the nodal forces can be related to the unknown coefficients as

$$\{\hat{F}_e\} = [C]\{a\}, \tag{22}$$

where $\{\hat{F}_e\} = \{\hat{V}_1 \ \hat{M}_1 \ \hat{V}_2 \ \hat{M}_2\}$, $\hat{V}_1 \equiv -\hat{V}(0)$, $\hat{M}_1 \equiv -\hat{M}(0)$, $\hat{F}_2 \equiv \hat{F}(L)$, $\hat{V}_2 \equiv \hat{V}(L)$, and $\hat{M}_2 \equiv \hat{M}(L)$ (see Figure 2). From Equations (21) and (22) we can obtain a relation between transformed nodal forces and displacements, similar to conventional FE,

$$\{\hat{F}_e\} = [C][B]^{-1}\{\hat{u}_e\} = [\hat{K}_e]\{\hat{u}_e\}, \tag{23}$$

where $[\hat{K}_e]$ is the exact elemental dynamic stiffness matrix. After the constants $\{a\}$ are known from the above equations, they can substituted back into Equation (20) to obtain the transformed displacements $\hat{w}, d\hat{w}/dx$ at any given x.

(23), corresponding to the perturbation solution, must be added to the particular solution, given by (19), to obtain total perturbation solution. Thus, we finally have two equations relating the transformed nodal forces to the transformed nodal displacements. For the perturbation solution, the boundary conditions for a cantilever beam are taken as

$$\hat{w}^1(0) = \frac{d\hat{w}^1}{dx}(0) = 0 \quad \text{and} \quad EI_0\frac{d^2\hat{w}^1}{dx^2}(L) = EI_0\frac{d^3\hat{w}^1}{dx^3}(L) = 0.$$

The other boundary conditions can be similarly implemented.

6. Numerical experiments

In this section, flexural wave propagation in a damaged beam, due to a narrow banded modulated pulse and a broad banded impulse loading, are studied and compared with the responses of the undamaged beam. In the first case of modulated pulse loading, the wave propagates nondispersively and the locations of the damage are obtained from the arrival time of the wave reflected from the notch. The wave speeds corresponding to the loading frequencies are obtained from the dispersion relation. This in turn helps in validation of the present formulation. Next, the flexural wave propagation due to broad band impulse load is studied for different damage parameters like width, ΔL, depth, h_d, and distance, L_d, from the free end or tip of the cantilever beam.

In all the cases the beam considered is an aluminum cantilever beam of length L, width $b = 0.05$ m, and depth $h = 0.01$ m. The material properties considered are Young's modulus, $E = 70$ GPa, Poisson's ratio, $\nu = 0.3$, and mass density $\rho = 2700$ kg/m^3. The order of the Daubechies scaling function used in all the examples is $N = 22$ unless otherwise mentioned.

First, the present method is validated by comparison with two-dimensional FE results. The comparison is made for the transverse wave velocity resulting from an impulse load of duration $500\,\mu$s and frequency content 4.4 kHz. The applied impulse load is very similar to that shown in Figure 3, however, there the impulse load has a duration of $50\,\mu$s and frequency content of 44 kHz, used for the numerical experiments
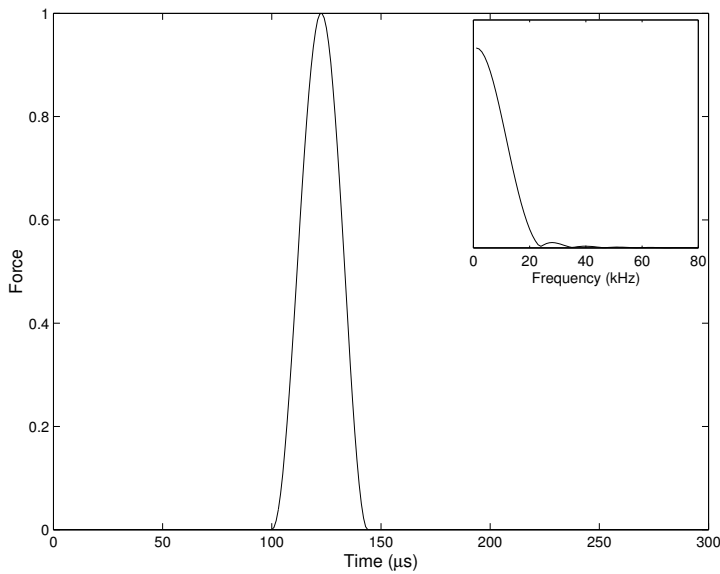
Figure 3. Impulse load in time and frequency (inset) domains.

presented in the later part of the paper. The responses simulated using the present method and two-dimensional FE modeling is presented in Figure 4 which shows the transverse velocity measured at the tip of a fixed-free beam with the impulse load applied at the tip. The damage is located at a distance of 0.5 m from the free end and has a depth of $h_d = 0.001$ m (10% of the depth of the beam) and width $\triangle L = 0.03$ m. The two-dimensional FE simulation is done using ANSYS 10.0, with 3994, 4-noded, plane stress quadrilateral elements and Newmark time integration with $\triangle t = 2\,\mu$s. As mentioned before, the WSFE results are obtained using only two elements with the intermediate node at the damage location. It
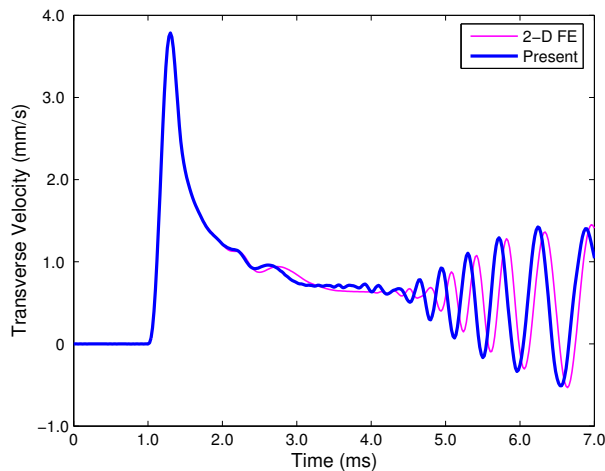

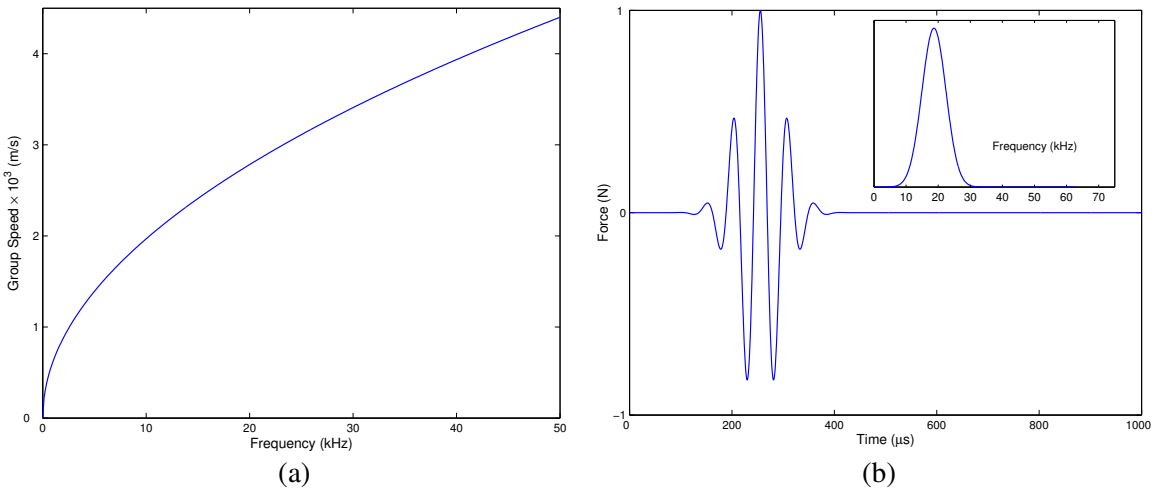**Figure 4.** Transverse velocities at the tip of a cantilever beam with notch.

Figure 5. Dispersion relation for (a) Euler–Bernoulli beam (left) and (b) modulated sinusoidal pulse load in time and frequency (inset) domains.

can be seen that the responses match very well. The frequency content of the applied load is consciously kept lower than that used for the other examples. This is because the two-dimensional FE modeling of the beam always simulates the results of Timoshenko beam theory and thus predicts lower wave speed than the Euler–Bernoulli beam theory used for the WSFE modeling. The difference in the responses due to this difference in the wave speeds is not negligible even in the slender beam case. However, the difference will be less for lower frequency excitation, hence a lower range of frequency is considered for the comparison between the two-dimensional FE and present models. The small difference in the wave speeds predicted by the two methods, observed in Figure 4, can be attributed to the reason explained above.

In Figure 5a, the dispersion relation for the beam, the group speed with respect to the frequencies, is plotted. The narrow banded modulated sinusoidal pulse is shown in time and frequency domains in Figure 5b. It can be seen that this load has a very narrow frequency band and propagates nondispersively, retaining its shape. Such a modulated pulse is widely used in health monitoring studies. Here, additional waves result due to reflection from the damage. The damage location is obtained from the arrival time of such a reflected wave, and the wave speed derived from the dispersion relation is shown in Figure 5a. In the present case, the modulated pulse has a central frequency of nearly $20\,\text{kHz}$, and the group speed of the flexural wave in the beam corresponding to this frequency is approximately $C_g = 2716\,\text{m/s}$, as calculated from Figure 5a. In Figure 6 the transverse velocities measured at the tip of the cantilever beam with length $L = 2.0\,\text{m}$, due to the modulated pulse applied at the tip in the transverse direction, are plotted. Figure 6 shows these velocities for beams with though-width notches at distances $L_d = 0.1, 0.25,$ and $0.4\,\text{m}$ from the free end, respectively. In all cases the notch width $\Delta L = 0.02$ and the depth $h_d = 10\%$ for the beam depth h. The arrival time of the waves reflected from the notch, as obtained from Figure 6, are, respectively, $T = 75, 185,$ and $300\,\mu\text{s}$. The locations of the damages, calculated inversely from these arrival times, and the group speed C_g are nearly equal to those assumed for the simulations, $L_d = 0.1, 0.25,$ and $0.4\,\text{m}$. This also validates the present formulation.
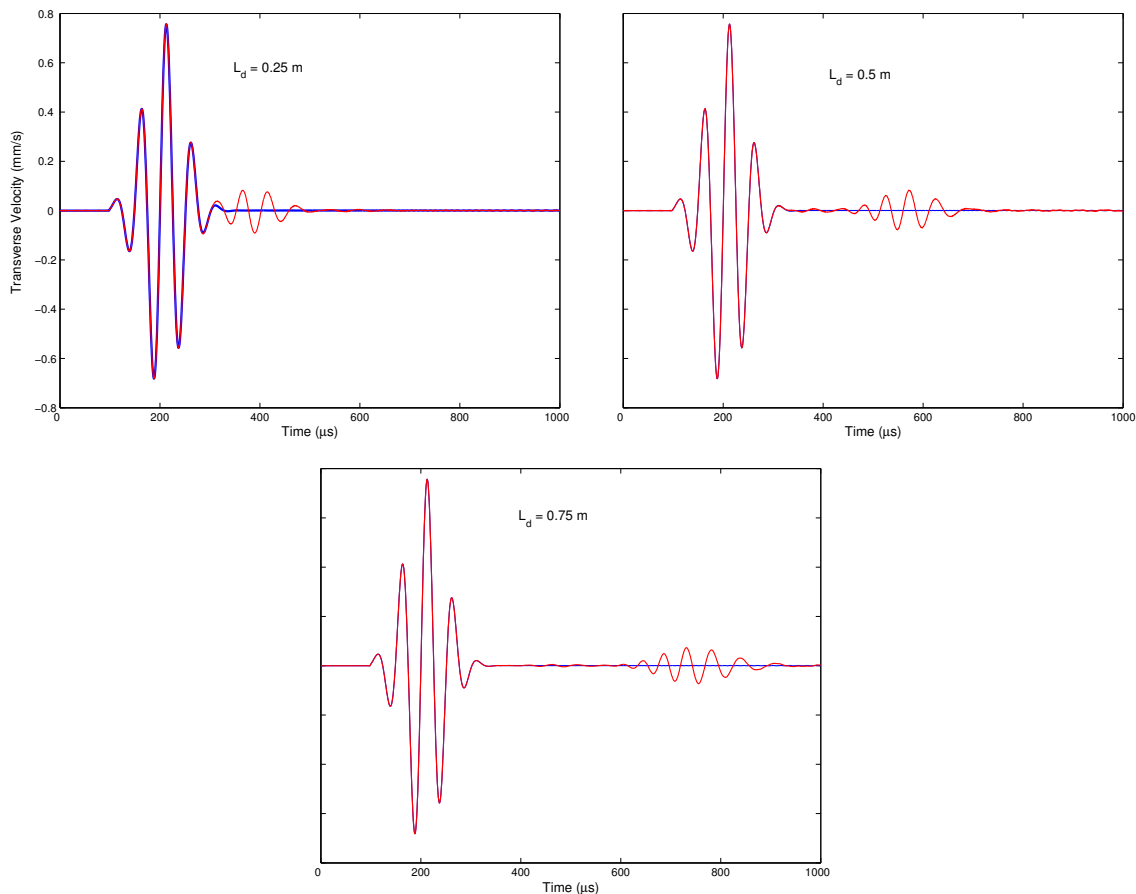
Figure 6. Transverse velocities at the tip of a cantilever beam of length $L = 2.0$ m with notch of $\Delta L = 0.02$ m, depth $h_d = 10\%$, at $L_d = 0.25$ m (upper left), $L_d = 0.5$ m (upper right), and $L_d = 0.75$ m (lower), compared with the response of an undamaged beam.

Next, examples are presented to study the effect of notch on the flexural wave propagation due to broad band impulse loading. The unit impulse load is shown in Figure 3 in time and frequency domains. The load has a time duration of $50\,\mu$s and a frequency content of 44 kHz. The load is again applied at the tip of a cantilever beam of length $L = 1.0$ m and the transverse velocities are measured at the tip. The effects of damage parameters, including damage width ΔL, depth h_d, and location L_d from the tip, on such responses are studied in the time and frequency domains. In Figure 7 the transverse tip velocities in three damaged beam configurations with varying damage width ΔL are plotted in the time and frequency domains, respectively. In all cases the notch is at a distance $L_d = 0.25$ m from the tip and the depth is $h_d = 0.1h$. The ΔL are varied as 0.01, 0.02, and 0.03 m. These responses are also compared with that of the undamaged beam. It can be seen from Figure 7a that the presence of the notch results in an early reflection of the flexural wave, which appears before the arrival of the wave reflected from the fixed end of the cantilever beam. In addition, the increase in ΔL results in an increase of the amplitude of the wave reflected from the notch. Similar responses are studied in frequency domain in Figure 7b. It can be

observed from the frequency domain response of the damaged and undamaged beams that the presence of notch results in a very small change only at the higher natural frequencies, while the amplitude changes considerably even at the lower frequencies. This is to be expected, since we are considering very small notch dimensions, length ΔL and depth h_d, consistent with the assumptions made in the perturbation analysis. The frequency responses are plotted in Figure 7b only within a small frequency range around 16.5 to 19.0 kHz. However, a small shift in the frequencies can also be observed at other frequencies. The figure shows that the increase in ΔL increases the amplitude and the shift in the frequency is nearly the same for all the damaged responses.

Figure 8 shows the responses of the damaged beam with different depths h_d of damage, with the other parameters, ΔL and L_d, remaining the same. In Figure 8a, the transverse velocities measured at the tip of the undamaged and damaged cantilever beams with a notch of $\Delta L = 0.01$ m at $L_d = 0.25$ m from the tip are presented. The depth of the notch is varied as $h_d = 0.1h, 0.2h$, and $0.3h$. Similar to the previous example, here the amplitude of the wave resulting from reflection from the notch increases with the increase in the depth h_d. In Figure 8b, the responses are plotted in the frequency domain. Even here, similarly to the previous example, a prominent change in the natural frequencies occurs at the higher values of 17.0 and 18.4 kHz. Interestingly, it can be seen that the pattern of the frequency response function within the plotted interval is very similar to that of the previous example. This is mainly because the damage model takes into account only the overall reduction in stiffness due to the notch, instead of the separate effect of h_d and ΔL.

Finally, numerical experiments are performed to study the responses of undamaged and damaged beams with the notch at different locations, due to the broad band impulse load (see Figure 3) applied at the tip in transverse direction. The transverse velocities measured at the tip are presented in Figure 9a. Here the notches have a width $\Delta L = 0.02$ m and depth $h_d = 0.1h$, but are located at distances $L_d = 0.1, 0.25$, and 0.4 m from the tip. It can be observed that for $L_d = 0.1$ m the reflection from the notch
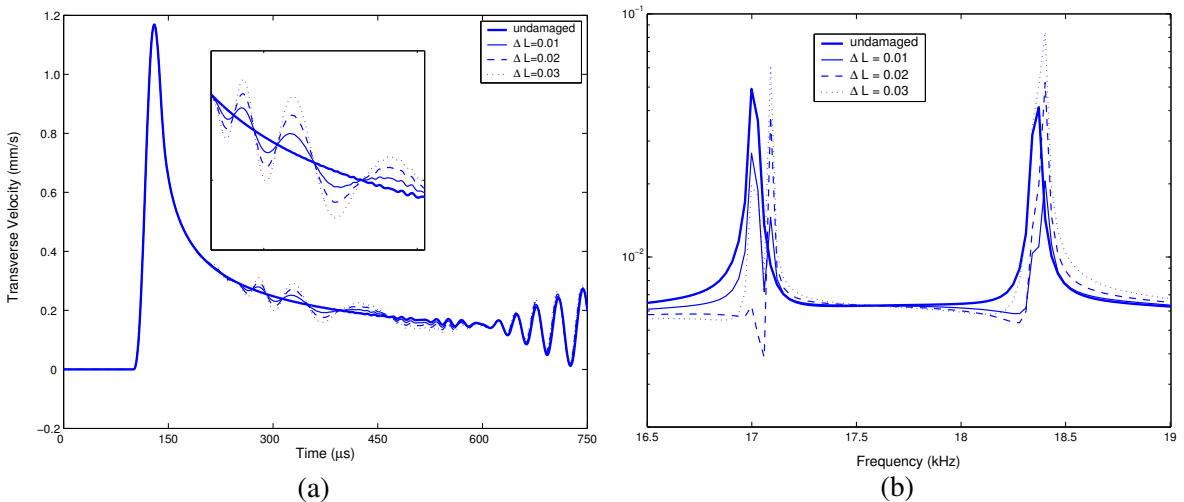

Figure 7. Transverse velocities at the tip of a cantilever beam of length $L = 1.0$ m with $L_d = 0.25$ m, $\Delta L = 0.01, 0.02$, and 0.03 m, and depth $h_d = 10\%$ compared with response of the undamaged beam in (a) time and (b) frequency domains.
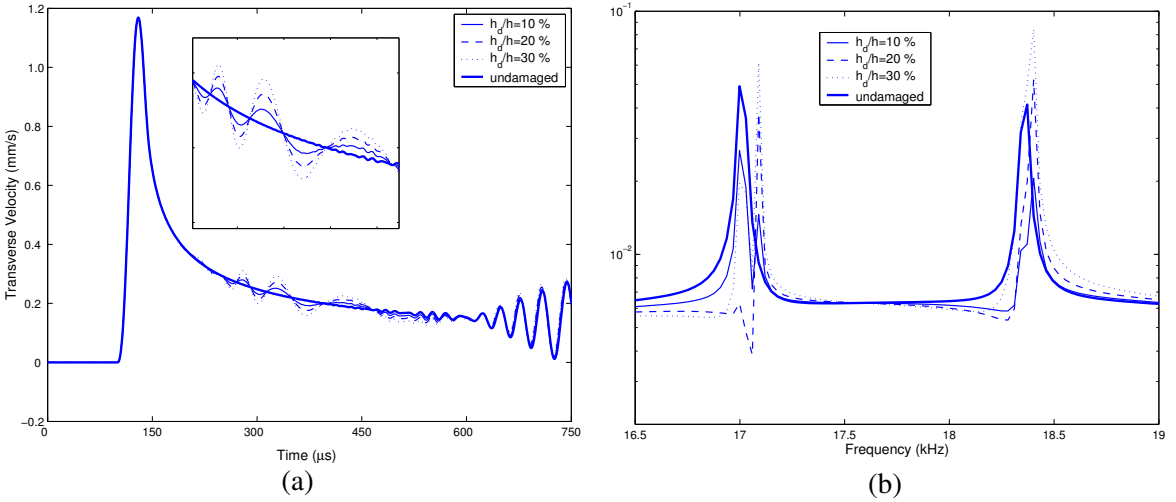
Figure 8. Transverse velocities at the tip of a cantilever beam of length $L = 1.0$ m with $L_d = 0.25$ m, $\Delta L = 0.01$ m, and depth $h_d = 10$, 20, and 30%, compared with the response of an undamaged beam in (a) time and (b) frequency domains.

arrives much earlier than expected. However, in the case of $L_d = 0.4$ m, the difference in the arrival time between the reflections from the damage and the fixed end is much less, and they are not quite distinguishable. In addition, for the same damage size, the amplitude of the reflection from the damage at $L_d = 0.4$ m is least. This is because the flexural waves are dispersive in nature, and thus the amplitude decreases as it travels more. The corresponding frequency domain responses are shown in Figure 9b, for frequency ranges around 21.5 kHz and 25 kHz respectively. In this case, unlike the two previous
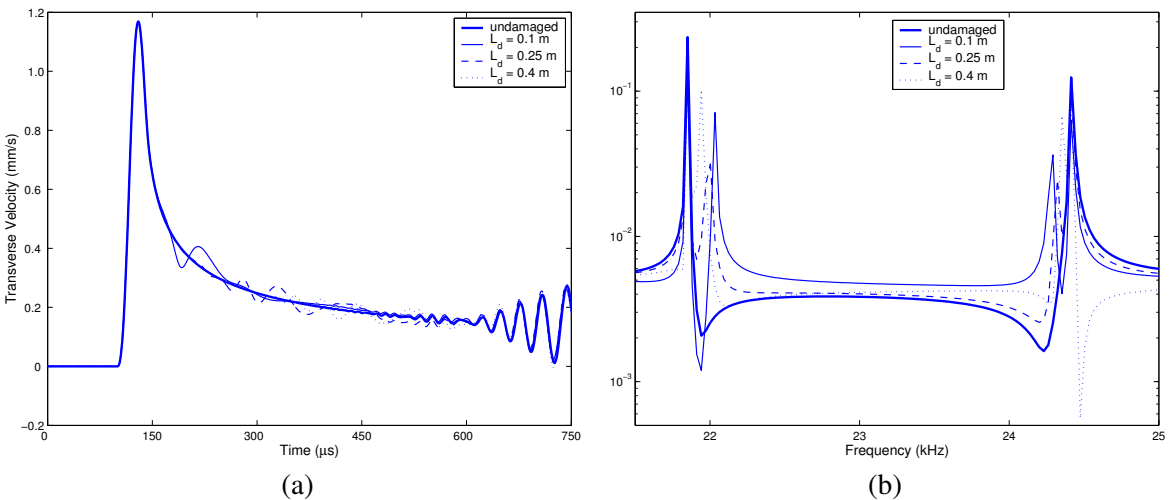

Figure 9. Transverse velocities at the tip of a cantilever beam of length $L = 1.0$ m with $L_d = 0.1$, 0.25, and 0.4 m, $\Delta L = 0.01$ m, and depth $h_d = 10\%$, compared with the response of an undamaged beam in (a) time and (b) frequency domains.

examples, considerable shift in frequencies occurs at two other frequencies, approximately 22.1 and 23.4 kHz.

7. Conclusions

In this paper, wave propagation characteristics in a damaged beam modeled as a Euler–Bernoulli beam with through-width notches are studied and compared with the response of the corresponding undamaged beam. The wave propagation of the notched beam is considered as a perturbation of the undamaged beam response with the assumption of small damage. The modeling is done using the wavelet based spectral finite element technique, including the perturbation solution. The wavelet based method allows efficient analysis of finite length structure due to the use of localized Daubechies scaling functions as bases, unlike the Fourier transform based spectral finite element method. Here the flexural wave propagation in the damaged beam is studied for both narrow and broad banded excitations in both time and frequency domains. For narrow banded modulated pulse loading the location of the damages, calculated inversely from the simulated response, using the arrival time and wave speeds obtained from the dispersion relations, matches very well with that considered for the simulation. Next, the effects of different damage parameters, including damage width, depth, and locations, on the response, due to broad band impulse loading, are analyzed in the time and frequency domains.

In the present work, coupling of axial and flexural modes due to the presence of damage is not considered. The model is developed for pure flexural wave propagation, neglecting the effect of axial mode conversion that may arise due to the damage. This is justified for damages with small dimensions, where this effect is negligible. However, further work lies in including such coupling in the formulation and studying its effects. It should also be mentioned that Timoshenko theory is more suited for the study of wave characteristics. However, the extension of the present method to Timoshenko theory will involve solution of a set of coupled partial differential equations, unlike Euler–Bernoulli beam theory. The formulation for a Timoshenko beam can be considered for future work.

References

[Beylkin 1992] G. Beylkin, "On the representation of operators in bases of compactly supported wavelets", *SIAM Journal of Numerical Analysis* **6**:6 (1992), 1716–1740.

[Chakraborty and Gopalakrishnan 2005] A. Chakraborty and S. Gopalakrishnan, "A spectrally formulated plate element for wave propagation analysis in anisotropic material", *Computer Methods in Applied Mechanics and Engineering* **194** (2005), 4425–4446.

[Daubechies 1992] I. Daubechies, *Ten lectures on wavelets*, CBMS-NSF Series in Applied Mathematics (SIAM, Philadelphia), 1992.

[Doyle 1999] J. F. Doyle, *Wave Propagation in Structures*, Springer, New York, 1999.

[Jones 1982] D. S. Jones, *The Theory of Generalized Functions*, Cambridge University Press, Cambridge, UK, 1982.

[Lestari 2001] W. Lestari, *Damage of composite structures : detection technique, dynamic response and residual strength*, Ph.D. thesis, Georgia Institute of Technology, 2001.

[Luo and Hanagud 1998] H. Luo and S. Hanagud, "An integral equation for changes in the structural characteristics of damaged structures", *International Journal of Solids and Structures* **34(35-36)** (1998), 4557–4579.

[Mitra and Gopalakrishnan 2005] M. Mitra and S. Gopalakrishnan, "Spectrally Formulated Wavelet Finite Element for Wave Propagation and Impact Force Identification in Connected 1-D Waveguides", *International Journal of Solids and Structures* **42** (2005), 4695–4721.

[Mitra and Gopalakrishnan 2006] M. Mitra and S. Gopalakrishnan, "Extraction of wave charateristics from wavelet based spectral finite element formulation", *Mechanical Systems and Signal Processing* **20** (2006), 2046–2079.

[Sharma et al. 2006] V. K. Sharma, M. Ruzzene, and S. Hanagud, "Perturbation methods for the analysis of the dynamic behavior of damaged plates", *International Journal of Solids and Structures* **43** (2006), 4648–4672.

[Williams and Amaratunga 1994] J. R. Williams and K. Amaratunga, "Introduction to wavelets in engineering", *International Journal for Numerical Methods in Engineering* **37** (1994), 2365–2388.

[Williams and Amaratunga 1997] J. R. Williams and K. Amaratunga, "A Discrete wavelet transform without edge effects using wavelet extrapolation", *Journal of Fourier Analysis and Applications* **3**:4 (1997), 435–449.

MIRA MITRA: mira@aero.iitb.ac.in
Department of Aerospace Engineering, Indian Institute of Technology, Bombay 400 076, India
http://www.aero.iitb.ac.in/~mira

S. GOPALAKRISHNAN: krishnan@aero.iisc.ernet.in
Department of Aerospace Engineering, Indian Institute of Science, Bangalore 560 012, India
http://www.aero.iisc.ernet.in/~krishnan

MASSIMO RUZZENE: Massimo.ruzzene@ae.gatech.edu
School of Aerospace Engineering, Georgia Institute of Technology, 270 Ferst Drive, Atlanta, GA, United States

NICOLE APETRE: nicole.apetre@gatech.edu
School of Aerospace Engineering, Georgia Institute of Technology, 270 Ferst Drive, Atlanta, GA, United States

S. HANAGUD: hanagud@ae.gatech.edu
School of Aerospace Engineering, Georgia Institute of Technology, 270 Ferst Drive, Atlanta, GA, United States